Scale Invariance of High Altitude Aircraft Observations in the Upper Troposphere and Lower Stratosphere at Tropical and Subtropical Latitudes

By S. J. HOVDE[1,2], K. K. KELLY[2], M. J. MAHONEY[3], M. H. PROFFITT[4], E. C. RICHARD[1,2], T. L. THOMPSON[2] and A. F. TUCK[2*]

1 *Cooperative Institute for Research in Environmental Science, University of Colorado, Boulder, Colorado, USA*
2 *Aeronomy Laboratory, National Oceanic and Atmospheric Administration, Boulder, Colorado, USA*
3 *Jet Propulsion Laboratory, California Institute of Technology, Pasadena, California, USA*
4 *World Meteorological Organization, Geneva, Switzerland*

SUMMARY

Exchange between the upper tropical troposphere and the lower stratosphere is considered by examining high altitude aircraft observations of water, ozone, methane, wind and temperature for scale invariance. Such scale invariance is indeed found, on scales from a few hundred metres to the maximum flown, 2800 km (25 great circle degrees). The results apply both to vertical exchange at the tropical tropopause and to isentropic exchange at the subtropical jet stream. All scales participate in the maintenance of the mean state, with substantial contributions from relatively infrequent but intense events in the long tails of the probability distribution functions. Past data are examined and found to fit the general framework. A unique mapping of tropical tropopause temperature to the total hydrogen content of the middleworld and overworld should not be expected.

KEYWORDS: Scale invariance Low latitudes Stratospheric-tropospheric exchange High altitude aircraft observations

1. INTRODUCTION

Richardson (1926) demonstrated that the dispersion of tracers in the atmosphere could not be described by true diffusion, but that it obeyed power law scaling; he suggested that the descriptor would need the characteristic of being everywhere continuous but nowhere differentiable, giving the Weierstrass function as an example. Such behaviour is now known as fractal (Mandelbrot 1983) and is associated with scale invariance and long-tailed probability distribution functions (Schertzer and Lovejoy 1985; Mandelbrot 1998); see also Turcotte (1997).

Recently, Methven and Hoskins (1998) showed the existence of a Kolmogorov capacity D_K, or box-counting dimension, of 0.43 for one-dimensional cuts through a potential vorticity spiral in a high resolution (T341, or about 30km) numerical simulation near the tropopause of an upper tropospheric cyclone. A related measure, the Hurst exponent H (Hurst 1951), has been evaluated for ozone, wind speed, wind direction, vertical wind speed and temperature by Tuck and Hovde (1999, a,b) for many flight segments of the ER-2 high altitude research aircraft in the lower stratosphere. The scaling extended from hundreds of metres to about 7000 km, or four orders of magnitude downwards from one Earth radius. The most frequent value of H for ozone was 0.57, consistent with the 0.43 value for the box-counting dimension; one would expect these to sum to unity in the absence of photochemistry. It has also been recently shown that persistent values ($H \geq 0.6$) for ozone are a signature that photochemistry is outpacing fluid mechanical mixing (Tuck *et al.* 1999).

As a prelude to the study of multifractality in these data, we have recently begun using the Hausdorff measure, H_1, as determined by the first order structure function, in lieu of the Hurst exponent. The relationship of the Hurst exponent, as calculated by a new algorithm, to the Hausdorff measure is given in the Appendix. The intention ultimately is to analyze for intermittency in the bifractal scheme of Davis and Marshak (1997) and to employ the universal 3-

parameter method of Schertzer and Lovejoy (1987).

In this paper, we apply the measures of scale invariance H and H_1 to observations of total water (vapour plus ice crystals detected as vapour) made at low latitudes from ER-2 and WB57F aircraft flying above, at and below the tropopause. Together with observations of ozone, methane, wind speed and temperature, the results are used to gain insight into any scale dependence that might be evident in exchange of air between the troposphere and the stratosphere in the tropics and subtropics. The long-tailed distributions in stratospheric water vapour reported by Helliwell *et al.* (1957) and Mastenbrook (1968) are interpreted, and confirmed in the light of modern results. Scale invariance generally will mean that all scales contribute and that a relatively small number of large amplitude events will have a substantial effect.

2. METHOD

We select all horizontal segments of all flights of ER-2 and WB57F aircraft which satisfy the following criteria: duration $\geq$ 3600 s and potential temperature $\theta \leq$ 420 K, with the exception of flights over tropical cyclones and hurricanes (three in number). This yields 4 segments from 4 flights of the ER-2, and 12 segments from 8 flights of the WB57F. The flight segments are specified in Table 1. Both aircraft cruise at Mach 0.7, or very close to 200 ms^{-1} for the flights used here. All data were analyzed at 1Hz except for the methane instrument which reported at 0.5 Hz.

MTP .06Hz

TABLE 1

Aircraft	Date yyyymmdd	Segment duration (s)	Coordinates (°lat, °lon)	Segment centre time (UTCs)	Approximate mean θ(K)
ER-2	19870131	5642	(8°S,130°E) (12°S, 130°E)	85895	365
ER-2	19870203	8721	(12°S,130°E) (18°S, 113°E)	92529	410
ER-2	19870814	7001	(6°N, 79°E) (10°S, 77°E)	48501	390
ER-2	19941026	7375	(14°N, 158°W) (0°, 158°W)	77830	415
WB57F	19980409	7017	(30°N, 95°W) (17°N, 84°W)	59535	370
WB57F	19980409	8064	(17°N, 84°W) (30°N, 95°W)	67972	415
WB57F	19980501	8209	(30°N, 95°W) (12°N, 95°W)	57963	360
WB57F	19980501	7314	(12°N, 95°W) (30°N, 95°W)	66224	370
WB57F	19980504	8835	(30°N, 95°W) (10°N, 95°W)	57627	385
WB57F	19980504	10363	(10°N, 95°W) (30°N, 95°W)	67225	410
WB57F	19980506	4822	(30°N, 95°W) (39°N, 92°W)	57231	355
WB57F	19980507	5144	(30°N, 92°W) (33°N, 84°W)	56911	370
WB57F	19980511	9119	(30°N, 95°W) (10°N, 95°W)	58482	375
WB57F	19980511	8052	(10°N, 95°W) (30°N, 95°W)	67907	415
WB57F	19990920	13607	(30°N, 95°W) (5°N, 95°W)	46709	365
WB57F	19990921	12323	(10°N, 82°W) (30°N, 95°W)	68272	360

Each flight segment was analyzed with the software described previously (Tuck and Hovde 1999a, b; Tuck *et al*. 1999). Here we consider total water, ozone, methane, horizontal wind speed and temperature. The calculation of the Hurst exponent was modified slightly, in a way which lessened its tendency to non-linearly amplify persistence; the effect of this was to give exponents for temperature H(T) closer to those for the other variables, rather than the most frequent value of 0.85 seen previously in first order. The other variables were little affected.

All variables showed scale invariance for all the flight segments, as gauged by linear log-log plots of the average range of the accumulated deviations vs. time sub-interval length. An example is shown in Fig. 1 for each variable during the 7314 s long flight segment of the WB57F on

19980501. This took place between (12°N, 95°W) and (30°N, 95°W) and was a flight path which followed the tropopause as accurately as possible, using real time feedback from the Microwave Temperature Profiler (Denning *et al.* 1989). Deviations of the aircraft from the tropopause altitude were generally less than 200 m, as illustrated in Fig. 2.

Since scale invariance is associated with long-tailed probability distribution functions, histograms were produced for all variables along all flight segments.

3. RESULTS

The values of the Hurst exponent obtained for each flight segment in Table 1 are displayed for total water, ozone, methane, windspeed and temperature in Table 2; each segment is uniquely identified by its duration in seconds, and the entries are in the same order as in Table 1. A hyphen entry indicates that no data were acquired. The methane instrument (Richard, private communication) was only operated on some of the WB57F flights.

TABLE 2

Segment duration(s)	$H(H_2O)$	$H(O_3)$	$H(CH_4)$	$H\left(\left[u^2+v^2\right]^{\frac{1}{2}}\right)$	H(T)
5642	0.53	0.48	-	-	0.52
8721	0.13	0.46	-	-	0.46
7001	0.12	0.29	-	0.47	0.49
7375	0.16	0.39	-	0.57	0.56
7017	0.24	0.30	-	0.40	0.63
8064	0.18	0.42	-	0.39	0.64
8209	0.55	0.37	0.36	0.52	0.58
7314	0.38	0.47	0.36	0.53	0.62
8835	0.37	0.53	-	0.51	0.62
10363	0.26	0.38	-	0.39	0.58
4822	0.53	0.56	0.36	0.60	0.63
5144	0.46	0.34	0.34	0.51	0.70
9119	0.31	0.25	-	0.49	0.58
8052	0.13	0.37	-	0.47	0.65
13604	0.35	0.36 (H_1)	0.19 (12,000 s)	-	0.58
12323	0.40	0.33 (H_1)	0.17 (7402 s)	0.48	0.60

The linearity of the log-log plots from which the values in Table 2 were obtained was in general excellent. These plots for the flight segments of lengths 7001 and 12323 seconds are illustrated in Figures 3 and 4 for water, along with the time series from which they were derived. The probability distributions are also plotted. It is noticeable that where there is very little variability in total water, such as the lower stratospheric 7001 s segment (Fig. 3), the value of H is very low, showing a high degree of antipersistence (negative auto-correlation) in the data on all scales. The probability distribution is also gaussian-like. These characteristics are an indication that for this segment, the water instrument's signal-to-noise ratio at 1 Hz is smaller than the (very low) level of atmospheric variability, and that the value of the power law scaling exponent is more an instrumental than an atmospheric earmark. Antipersistent (low) values of $H(H_2O)$ are also found for the 8721, 7375,

8064 and 8052 s segments but no others, which are better typefied by the 12323 s segment illustrated in Fig. 4. In these cases, the water mixing ratio is larger than the 3-6 ppmv of the five most antipersistent cases, and is also more variable. The scaling is now characteristic of the atmosphere, and is generally similar to that of the ozone. The first order structure function was evaluated for the data shown in Figures 1, 3, and 4, and the results are plotted in the centre log-log plots as the square symbols (log(Moment)). In the case of water, the change in slope at about 30s is a scale break and reflects the scale at which instrument noise becomes greater than atmospheric variability. This is also true for methane at a scale of about 100s in Fig. 1. The methane scaling for the 13604 s and 12323 s (Fig. 4) segments gave values of H of 0.19 and 0.17, respectively, which reflects the fact that at constant pressure (about 120 hPa) below the tropical tropopause, the true tropospheric variability is somewhat smaller than the instrument noise. Both are very low; the methane still, however, shows real atmospheric correlation with the ozone. In the case of wind speed and temperature, there is a probable indication of multifractal behaviour. Figure 5 shows the structure function variograms and the plots of H_q against q for ozone, wind speed, and temperature for the 7314s flight segment. While the ozone displays H_q = constant $\approx$0.30, this is not true for the wind speed and temperature, which are likely therefore to be multifractal. This behaviour will be explored in future work. Irrespective of location relative to the tropopause, the data collectively illustrate that in the range $350 \leq \theta \leq 420$ K there is scale invariance in total water, ozone, methane, wind speed and temperature. This was true whether using the Hurst exponent or the Hausdorff exponent evaluated from structure function analysis. The invariance extends over flight tracks from 6 to 25 great circle degrees in length, down to a few hundred metres. The associated histograms have long tails.

It is also of interest to consider the values of water and methane measured along the tropical tropopause on 19980501, see Figures 1 and 2. There is no obvious phase relationship between them, and the values of both vary, even away from the segment of flight track saturated with respect

to ice (64100 to 66600 s).

There have been consistent reports of high, >10 ppmv and up to 80 ppmv on occasion, episodic values of water vapour above the tropopause in mid-latitudes of the northern hemisphere during Meteorological Research Flight Canberra operations, detected as excursions from sequences of more normal, lower values (Helliwell *et al*. 1956; Cluley and Oliver 1979; Foot 1984). A similar record exists for a balloon-borne frostpoint hygrometer which normally recorded low values (Mastenbrook 1968). There is one account (Roach 1962) of values of water > 10 ppmv and of ozone in the range $100 < O_3 < 1500$ ppbv well above the tropopause on the Canberra flight track from 50°N to 68°N near the Greenwich meridian on 19620206. In Fig. 6, we redraw those observations along with the flights of 19620131 and 19620201, with units of ppmv for water and ppbv for ozone. All three are in the range 350 to 390 K, and are above the tropopause. The flight of 19620201 has low water and high ozone, unequivocally stratospheric characteristics. The other two however show upper tropospheric water and low but stratospheric ozone. The ER-2 flight of 19890207 (Fig. 7) shows a similar population characterizing air in the range $340 < \theta < 420$ K as having stratospheric ozone (100 - 1000 ppbv) accompanied by upper tropospheric water (up to 25 ppmv) near (60°N, 6°E). Such air can only have been obtained by mixing between lower stratospheric and upper tropospheric elements; grand average profiles over scores of profiles by the ER-2 between 1987 and 1996 reveal this to be the case (Reid *et al*. 2000). Back trajectories using the NOAA-NCEP re-analysis from the ER-2 flight of 19890207 confirm the origin of the mixed air on the cyclonic side of the subtropical jet stream over N. Africa (Fig. 8). We note that the 4822 s section of WB57F flight on 19980506 was flown just above the tropopause at latitudes immediately north from the subtropical jet stream core and contains air with ~500 ppbv of ozone accompanied by ~15 ppmv of water (Fig. 9). The NOAA-NCEP reanalyzed potential vorticity maps for the Meteorological Research Flight Canberra flights on 19620131 and 19620206 similarly confirm the subtropical origin, in this case from the Mexican Gulf and Atlantic sectors respectively (Fig. 10).

By contrast, the the PV map for 19620201 shows the polar vortex extending south along the Greenwich meridian to the Bay of Biscay, explaining the low water, high ozone air seen by the aircraft; it was flying in the highest PV air in the whole vortex on its track along the Greenwich meridian to 68°N. Points from three ER-2 flights from January 1989 over Scandinavia during undisturbed conditions are plotted with those from the disturbed flight of 19890207 and the three 1962 Canberra flights in Fig. 11. The presence of air with upper tropospheric water and lower stratospheric ozone is evident during disturbed conditions in both 1962 and 1989, and is similarly absent from the vortex or near vortex air encountered in undisturbed conditions in both years.

The presence of air containing lower stratospheric ozone and upper tropospheric water on the immediately cyclonic side of the subtropical jet stream on 19980506 (Fig. 9) thus confirms the validity of the earlier measurements, and directly shows the subtropical jet stream to be a mixing and exchange zone, as proposed by Brewer (1960), Murgatroyd (1965), Allam and Tuck (1984), Foot (1984), Dessler *et al.* (1995) and Tuck *et al.* (1997). This view is reinforced by the 5144 s segment flown by the WB57F on 19980507. The flight track was diagonally across the subtropical jet stream as a segment of a line running from the right entrance towards the left exit, isentropically at 370 K. Figure 12 shows the wind speed and water traces; consistent with the scale invariance in both, there is substantial variability on all scales; it is clear from the water that there is exchange across the core. Recent work (Vaughan and Timmis 1998; O'Connor *et al.* 1999; Reid *et al.* 2000) has shown explicit examples of such transport from the subtropical jet region to midlatitudes in the context of Lagrangian and PV analyses from global numerical weather prediction suites. The scaling on the 4822 s segment in Fig. 9 is close to random for all variables, a further indication of active mixing. The long-tailed distributions seen by Helliwell *et al.* (1957) and Mastenbrook (1968) in lower stratospheric frost point observations are consistent with the analysis, and indeed are an inevitable adjunct of scale invariant (fractal) behaviour (Mandelbrot 1998; Schertzer and Lovejoy 1985; Turcotte 1997).

4. DISCUSSION AND CONCLUSIONS

Flights in the range $350 < \theta < 420$ K at latitudes in the band from 12°S to 39°N have universally shown fractal behaviour, with the concomitant scale invariance and long-tailed probability distributions in ozone, total water, methane, windspeed and temperature. The range of potential temperatures spans the scale-height centred on the tropical and subtropical tropopause; Figure 13 shows a scatterplot of the tropopause θ_{TROP} versus latitude for the flights. The remarkable feature that for each individual flight θ_{TROP} is lower near the equator and higher near the subtropical jet stream by 10 - 20 K (typically 365-395 K in the inner tropics, 370-420 K on the immediate anticyclonic side of the jet maximum) probably reflects the mixing of potentially warm air from the lower midlatitude stratosphere up the isentropes towards and into the inner tropics. Such motion will tend to destabilize the air with respect to vertical air parcel motion and so raise the tropopause. The measurements of ozone, methane and water are consistent with such air motion. In all cases, including the inner tropics, the tropopause is at a higher value of potential temperature than that equivalent to the highest observed moist static energies at the tropical surface, some 355 K.

The scale invariance implies, for example, that along a typical 10 000 s flight track (2000 km) there will be one event with relative amplitude of order 10^4, 10 with 10^3, 100 with 10^2, 1000 with 10 and 10000 with unity. The conclusion is, that when stratosphere-troposphere exchange and mixing occur along the tropical tropopause and at the horizontal boundary formed by the subtropical jet stream, this is the probability distribution as a function of length scale which will be involved. Figure 14 shows the behaviour of methane and water during a long flight from Hawaii (20°N, 158°W) to Fiji (18°S, 178°E) at $440 < \theta < 470$ K. In the inner tropics, there is a shotgun relation between methane and water, with the latter varying in a range of 1.3 ppmv centred on a mean of 4.3 ppmv; there is no clear one-to-one relationship well above the inner tropical tropopause. Comparatively rare, relatively intense events may have substantial influence, and accordingly a

unique mapping of the total hydrogen content crossing the tropopause on to the content of the "overworld" (the stratosphere above about 50 hPa in the tropics and above about 100 hPa in the extratropics) would not be expected. Instead, it is determined by the interplay of subtropical jet stream dynamics and inner tropical ascent via deep convection over the annual cycle in the range $350 < \theta < 500$ K, with whatever their resultant is at about 50 hPa in the inner tropics being the content of what enters the overworld. There is no single "entry level" value of total hydrogen at the tropical tropopause. Recirculation (Tuck *et al*. 1997), working through the dynamics associated with the subtropical jet stream, is in evidence in the "middleworld"; there is a further implication that interpreting observed trends in stratospheric water and methane will not be as simple as diagnosing tropopause temperature. Scale invariance implies participation of all scales in mixing and exchange, and that relatively infrequent but high amplitude events contribute substantially to the maintenance of the mean state.

ACKNOWLEDGEMENT

We thank Dr. S. J. Reid for Fig. 7 and Dr. G. Kiladis for Fig. 9.

APPENDIX

Self-Affinity

In fractal geometry, the self-similarity of an object is expressed mathematically by the power law relation $N = \frac{C}{r^{D_f}}$, where N is the number of fragments of the object with characteristic linear dimension r, C is a constant of proportionality, and D_f is the fractal dimension (which may be equal to the Euclidean dimension of the object). A self-similar object exhibits scale-invariance, which means that the appearance of the object is independent of the scale at which it is examined. Strictly self-similar objects are called deterministic fractals, whereas objects that are not strictly self-similar but nonetheless can be characterized by the power law relation are called statistical fractals. An example is a map of rocky coastline. Calculating the fractal *box* or *capacity* dimension of the coastline involves determining the (ideally minimal) number N_i of square boxes of linear dimension r_i that are needed to cover the coastline. This is done for a number of different r_i and then D_f is found to be the slope of the line fit through the points $(\log r_i, \log N_i)$.

Self-similar fractals, both deterministic and statistical, are necessarily isotropic, meaning that the fractal dimension D_f does not depend on the geometrical orientation of the box covering with respect to the object. In the case of the rocky coastline, the counts, N_i, do not depend on the orientation of the boxes (as long as they are all oriented in the same direction), since the coastline scales in the same manner in both the x- and y-directions. Mathematically this concept can be expressed (in two dimensions) as the fact that $f(x,y)$ is statistically similar to $f(rx,ry)$, where r is a scale factor.

Self-affinity is the term used when there is scale-invariance but direction matters. An example is the earth's topography in three dimensions: the elevation scales differently than the horizontal coordinates. Another example is the graph of any scale-invariant function where the abscissa and

ordinate have different units. For example, if $F(t)$ is a scale-invariant function of t, and $R_F(\tau)$ is the range of F over a t-interval τ, and r is a scale factor, then $R_F(r\,\tau)$ is proportional to $r^{Ha}R_F(\tau)$, where Ha is called the Hausdorff measure. That is, the set of points $(t,F(t))$ is statistically similar not to $(rt,rF(t))$, but to $(rt,r^{Ha}F(t))$. The anisotropy is captured by the fact that the scale factors are different for the two coordinates.

In practice, the Hausdorff measure is determined by finding $R_F(r_i\,\tau)$ for different r_i and then fitting a line through the points ($\log r_i$, $\log R_F(r_i\,\tau)$), with Ha being the slope of this line. The fractal box dimension of F can then be computed from Ha as follows (Feder 1988): Let $r_i\tau$ be the width of a box, and let $r_i h$ be the height of the box. Then, if the graph of F extends from $t = 0$ to $t = T$, the number of boxes needed to cover the graph will be on the order of $N_i = \left(\frac{T}{r_i\tau}\right)\left(\frac{\overline{R_F(r_i\tau)}}{r_i h}\right)$,

where the overbar denotes average. But $R_F(r\,\tau) \propto r^{Ha}R_F(\tau)$, since F is scale invariant. Therefore, $N_i \propto \left(\frac{T}{r_i\tau}\right)\left(\frac{r_i^{Ha}R_F(\tau)}{r_i h}\right) \propto r_i^{Ha-2}$. Comparison with the power law relation for isotropic fractals, $N = \frac{C}{r^{D_f}}$, yields the following definition for the fractal dimension of F: $D_f = 2 - Ha$

Structure Function Analysis

Structure functions in a multifractal formalism were developed by Frisch and Parisi (1985). Given a function $F(t)$, the q-th order structure function of F is the function $M_q(\tau)$ that is the q-th

order absolute moment of F over increment τ.

$$M_q(\tau) = \left\langle |F(t+\tau) - F(t)|^q \right\rangle$$

The angled brackets denote the average over all appropriate t. That is, if the domain of F is [0,T], then "appropriate" t for a given τ would be $0 \le t \le T - \tau$. Note that $M_1(\tau)$ is equivalent to $\left\langle R_F(\tau) \right\rangle$. So, if F is self-affine, then $M_1(\tau) \propto \tau^{Ha}$.

Structure functions provide an ideal transition to multi-fractal analysis since the scaling exponent obtained from the first order structure function is equivalent to the Hausdorff measure and the exponents obtained from successive orders indicate the level of multi-fractality that is present. The scaling exponent is normally represented as a function of q, $\zeta(q)$, and then H_q is defined to be $\zeta(q)/q$. Therefore, $H_1 = \zeta(1) = Ha$. In the case where $F(t)$ is turbulent velocity, Kolmogorov (1962) found that $H_3 = \zeta(3)/3 = 1/3$.

For a monofractal signal, all of the H_q are equal; that is $\zeta(q)/q$ is constant.

Rescaled Range Analysis

Rescaled range analysis is another way to characterize the scale-invariance of a function $F(t)$, but it focuses on the first differences of F, $D(t)$, rather than on F itself. H. E. Hurst (1951) developed the method back in the late 1940's when he was trying to determine what height of the yet-to-be-built High Aswan Dam would be adequate to control the flow of the Nile River. He had at his disposal over a thousand years' of Nile River data. The following concise description of his method is due to Bassingthwaighte and Raymond (1994).

Over some time interval τ, $Q(t)$ represents the flow of water into the reservoir. The outward flow is assumed to be the average of the inward flow: $\overline{Q} = \frac{1}{\tau}\int_0^\tau Q(\theta)d\theta$. At any given time t within

the interval τ, the volume of water contained within the reservoir is given by $V(t) = V(0) + \int_0^t Q(\theta)d\theta - t\,\overline{Q}$. The range of V is $R(\tau) = V_{max}(\tau) - V_{min}(\tau)$. This range is normalized by the standard deviation of Q over the interval: $S(\tau) = \left(\frac{1}{\tau}\int_0^\tau (Q(\theta) - \overline{Q})^2 d\theta\right)^{\frac{1}{2}}$. Hurst found empirically that the normalized ("rescaled") range was related to the interval τ by a power law: $\frac{R(\tau)}{S(\tau)} \propto \tau^H$. The scaling exponent, H, is now known as the Hurst exponent.

In practice, if $F(t)$ is the signal of interest and is defined on the interval $[0,T]$, the first step is to generate the first differences of F, $D(t)$. The rescaled range analysis is then carried out using D as Q. The interval $[0,T]$ is divided into halves so that $\tau_1 = [0,T/2]$ and $\tau_2 = [T/2,T]$. R/S is calculated for each τ_i and then the two quantities are averaged. This yields the first point on a plot of $log\left\langle\frac{R(\tau)}{S(\tau)}\right\rangle$ versus log τ. The process is repeated by continually subdividing the intervals. As τ becomes smaller, there are more values of R/S to average. If $F(t)$ is self-affine, the points on the log-log plot will lie on a line, the slope of which is H.

In Hurst's original formulation, the quantity $\overline{Q}$ came not from averaging over the interval τ, but from averaging over the entire domain of the data. That is, it was a *global* – rather than *interval* – average. The use of the interval average is now referred to in the literature as "trend removal" because the effect is to filter out local trends that necessarily become more pronounced as the interval length decreases. As Bassingthwaighte and Raymond note, Hurst introduced trend removal and Mandelbrot recommends its use, but the authors themselves, apparently skeptical, undertook a

comparison of analyses with and without trend removal and found that including trend removal improved the estimate of H only for signals with H greater than about *0.6*. The present authors have verified those results and, in addition, note that the use of trend removal does not significantly change values of H below 0.6, and so now it is our practice to always employ trend removal when doing rescaled range analysis.

Relationship Between H and H_1

From the descriptions of the respective methods, it is not at all obvious that the Hurst exponent H and the scaling exponent H_1 obtained from the first order structure function are related. Indeed, the connection is made, not in the space of the self-affine signals themselves, but in the space of their Fourier transforms, through the spectral exponent, β. Turcotte (1997) gives the following explanation of the relationship between β and H_1.

For a function $F(t)$ defined on some interval $0 \le t \le \tau$, the Fourier transform of F is given by $Y(f,\tau) = \int_0^\tau F(\theta) e^{2\pi i f\theta} d\theta$ and the power spectral density of F is given by $PSD(f) = \frac{1}{\tau}|Y(f,\tau)|^2$. If F is a self-affine fractal, then the power spectral density has a power law dependence on frequency: $PSD(f) \propto f^{-\beta}$. This is where the spectral exponent appears. Now suppose F_1 and F_2 are related by $F_2(t) = \frac{1}{r^{H_1}} F_1(t)$. The Fourier transform of F_2 is given by $Y_2(f,\tau) = \int_0^\tau F_2(\theta) e^{2\pi i f\theta} d\theta = \int_0^{r\tau} \frac{F_1(\theta')}{r^{H_1}} e^{2\pi i f\theta' / r} \frac{d\theta'}{r}$, where $\theta' = r\theta$. Thus, $Y_2(f,\tau) = \frac{1}{r^{H_1+1}} Y_1\left(\frac{f}{r}, r\tau\right)$ and $PSD_2(f) = \frac{1}{\tau}|Y_2(f,\tau)|^2 = \frac{1}{r^{2H_1+1}} PSD_1\left(\frac{f}{r}\right)$. Now observe that F_2 is simply a properly rescaled

version of $F_1 = F$. That is, F_1 and F_2 are both realizations of F at different scales. The subscripts can thus be dropped and the power law dependence of the power spectral density on frequency becomes $PSD(f) = \frac{1}{r^{2H_1+1}} PSD\left(\frac{f}{r}\right)$. It follows that $\beta = 2H_1 + 1 = 5 - 2D_f$. The graph of a self-affine function should have fractal dimension $1 < D_f < 2$ and $0 < H_1 < 1$. Therefore, $1 < \beta < 3$.

Now what remains is to find the relationship between β and H. An important preliminary result , not reproduced here, is that for Gaussian white noise, $H = \frac{1}{2}$ (Mandelbrot, 1969). This fact, together with the observation that $\beta = 0$ for Gaussian white noise , leads to the relation $\beta = 2H - 1$. Note, however, that since $\beta = 0$ is not in the range $(1,3)$, the graph of Gaussian white noise is not self-affine. However, the integral of Gaussian white noise becomes Brownian motion with spectral exponent $\beta = 2$. This is consistent with the fact that rescaled range analysis is applied to the first differences of the signal in question. (The set of first differences of Brownian motion is Gaussian white noise.) Thus, letting F denote the self-affine function of interest, and letting D denote the first differences of F, the relationship between H and H_1 is given by $\beta^F = 2H_1{}^F + 1 = \beta^D + 2 = 2H^D + 1$, and so $H_1{}^F = H_D$, which means that the Hausdorff measure for a self-affine function should be equivalent to the Hurst exponent of the underlying differences.

Note that Mandelbrot (1983) extended these analyses from strictly Brownian motion ($\beta = 2$) to *fractional* Brownian motion ($1 < \beta < 3$). However, Bassingthwaighte and Raymond, and Turcotte have shown empirically that rescaled range analysis is biased for very persistent or very anti-persistent signals. Therefore, we believe that the method should not be used as a means to calculate fractal dimension. We continue to investigate, however, its striking ability to produce straight line log-log plots for noisy data when the Hausdorff measure, due to its sensitivity, fails to do so. (See,

for example, Fig. 1(c).)

REFERENCES

Allam, R. J. and Tuck, A. F. 1984 Transport of water vapour in a stratosphere-troposphere general circulation model. II: Trajectories, *Q.J.R. Meteorol. Soc.*, **110**, 357-392

Bassingthwaighte, J. B. and Raymond, G. M. 1994 Evaluating rescaled range analysis for time series, *Ann. Biomed. Eng.*, **22**, 432-444

Brewer, A. W. 1960 The transfer of atmospheric ozone into the troposphere, MIT Planetary Circulation Project; presented to the United Nations Committee on the Effects of Radiation, New York, January 1960.

Cluley, A. P. and Oliver, M. J. 1979 An observation of unusually high humidity in the stratosphere, *Q.J.R. Meteorol. Soc.*, **105**, 306-309

Davis, A. B. and Marshak, A. 1997 Interactions: Solar and laser beams in stratus clouds, fractals & multifractals in climate & remote-sensing studies, *Fractals*, **5**, 129-166

Denning, R. F., Guidero, S. L., Parks, G. S. and Gary, B. L. 1989 Instrument description of the airborne Microwave Temperature Profiler, *J. Geophys. Res.*, **94**, 16757-16766

Dessler, A. E., Hintsa, E. J. Weinstock, G. M., Anderson, J. G. and Chan, K. R. 1995 Mechanisms controlling water vapor in the lower stratosphere: "a tale of two stratospheres", *J. Geophys. Res.*, **100**, 23167-23172

Feder, J. 1988 *Fractals*, Chapter 10, Plenum Press

Foot, J. S. 1984 Aircraft measurements of the humidity in the lower stratosphere from 1977 to 1980 between 45°N and 65°N, *Q.J.R. Meteorol. Soc.*, **110**, 303-319

Helliwell, N.C., Mackenzie, J. R., and Kerley, M.J. 1957 Some further observations from aircraft of frost point and temperature up to 50 000 ft., *Q.J.R. Meteorol. Soc.*, **83**, 257-262

Hurst, H. E. 1951 Long term storage capacity of reservoirs, *Trans. Am. Soc. Civ. Eng.*, **116**, 770-808

Kolmogorov, A. N. 1962 A refinement of previous hypothesis concerning the local structure of turbulence in viscous incompressible fluid at high Reynolds number, *J. Fluid Mech.*, **13**, 82-85

Mandelbrot, B. B. and Wallis, J. R. 1969 Robustness of the rescaled range R/S in the measurement of noncyclic long run statistical dependence, *Water Resour. Res.*, **5**, 967-988

Mandelbrot, B. B.	1983	*The Fractal Geometry of Nature*, Chapter IX, W. H. Freeman, New York
Mandelbrot, B. B.	1998	*Fractals and 1/f Noise*, Chapter N15, Springer-Verlag, New York
Mastenbrook, H. J.	1968	Water vapor distribution in the stratosphere and high troposphere, *J. Atmos. Sci.*, **28**, 1495-1501
Methven, J. and Hoskins, B. J.	1998	Spirals in potential vorticity. Part I: Measures of structure, *J. Atmos. Sci.*, **55**, 2053-2066
Murgatroyd, R. J.	1965	Ozone and water vapour in the upper troposphere and lower stratosphere, pp 68-94, in *Meteorological Aspects of Atmospheric Radioactivity*, WMO, No. 169, Geneva
O'Connor, F. M., Vaughan, G. and de Backer, H.	1999	Observation of sub-tropical air in the European midlatitude lower stratosphere, *Q.J.R. Meteorol. Soc.*, **125**, 2965-2986
Parisi, G. and Frisch U.	1985	A multifractal model of intermittency, in *Turbulence and Predictability in Geophysical Fluid Dynamics*, North-Holland, Amsterdam, ed. M. Ghil, R. Benzi, G. Parisi
Reid, S. J.,Tuck, A. F. and Kiladis,G.	2000	On the changing abundance of ozone minima in midlatitudes, *J. Geophys. Res.*, **105**, in press
Richard, E.C.	2000	Private Communication
Richardson, L. F.	1926	Atmospheric diffusion shown on a distance-neighbour graph, *Proc. Roy. Soc.*, **A110**, 709-737
Roach, W.T.	1962	Aircraft observations in the lower sub-arctic stratosphere in winter, *Meteorological Research Committee Paper* **121** (available:National Meteorological Library,Meteorological Office, Bracknell)
Schertzer, D. and Lovejoy, S.	1985	The dimension and intermittency of atmospheric dynamics, pp 7-33, *Turbulent Shear Flows*, **4**, Springer, New York
Schertzer, D. and Lovejoy, S.	1987	Physical modeling and analysis of rain clouds by anisotropic scaling multiplicative processes, *J. Geophys. Res.*, **92**, 9693-9714

Tuck, A. F., Baumgardner, D., Chan, K. R., Dye, J. E., Elkins, J. W., Hovde, S. J., Kelly, K. K., Loewenstein, M., Margitan, J. J., May, R. D., Podolske, J. R., Proffitt, M. H., Rosenlof, K. H., Smith, W. L., Webster, C. R. and Wilson, J. C.	1997	The Brewer-Dobson circulation in the light of high altitude in situ aircraft observations, *Q.J.R. Meteorol. Soc.*, **123**, 1-69
Tuck, A. F. and Hovde, S. J.	1999a	Fractal behaviour of ozone, wind and temperature in the lower stratosphere, *Geophys. Res. Lett.*, **26**, 1271-1274
Tuck, A. F. and Hovde, S. J.	1999b	An examination of stratospheric aircraft data for small scale variability and fractal character, pp 249-254, Air pollution research report 69, *Mesoscale Processes in the Stratosphere*, EUR 18912 EN, EC, Brussels
Tuck, A. F., Hovde, S. J. and Proffitt, M. H.	2000	Persistence in ozone scaling under the Hurst exponent as an indicator of the relative rates of chemistry and fluid mechanical mixing in the stratosphere, *J. Phys. Chem. A*, **103**, 10445-10450
Turcotte, D. L.	1997	*Fractals in Geology and Geophysics*, 2nd edition, Cambridge University Press, Cambridge
Vaughan, G. and Timmis, C.	1998	Transport of near tropopause air into the lower midlatitude stratosphere, *Q.J.R. Meteorol. Soc.*, **124**, 1559-1578

FIGURE CAPTIONS

Figure 1. The instrumental time trace, the log-log plot for the Hurst exponent (round symbols, solid line in centre plot) and the associated histogram for the WB57F flight 7314 s in length (table 1), 19980501. (a), water; (b), ozone; (c), methane; (d), wind speed; (e), temperature. The square symbols and dashed line are the first order structure functions; see also figure 5.

Figure 2. The isentrope curtain from the Microwave Temperature Profiler above and below the WB57F flight segment corresponding to figure 1. The flight track and the tropopause are marked; the aircraft was flown along the tropopause based on feedback from the MTP into the cockpit.

Figure 3. Same as for figure 1, but for the 7001 s leg of the ER-2 on 19870814; methane was not measured on this flight.

Figure 4. Same as for figure 1, but for the 12323 s leg of the WB57F on 19990921.

Figure 5. Structure functure variograms (left side) and plots of H(q) vs q (right side) for the same 7314 s segment illustrated in figure 1.

Figure 6. Water vapour and ozone along Canberra flight track 55°N-68°N near the Greenwich meridian. Wind speed and direction are conventional for the fleches; the plain number is water volume mixing ratio in ppmv, that in square brackets is ozone, ppbv. (a) 31 January 1962, (b) 01 February 1962, (c) 06 February 1962. All flights were approximately centred on local noon.

Figure 7. Profiles of water and ozone following ER-2 take-off from Stavanger (59°N, 6°E) on 19890207. Note the values of ozone and water at $\theta \leq 420$ K. The tropopause was at $\theta = 330$ K.

Figure 8. Back trajectories at θ = 390 K, from the profiles in figure 7. The air at 390 K originated from the N. Africa-Arabia sector, near the subtropical jet stream; it contains about 50 ppmv of water and about 300 ppbv of ozone, i.e. it is a mixture of upper tropospheric and lower stratospheric air.

Figure 9. The 4822 s segment from the WB57F flight of 19980506. The ozone and water traces were taken just above the tropopause, on the cyclonic side of the subtropical jet stream core. The joint distribution of water (10-15 ppmv) and ozone (200 - 500 ppbv) is evidence of mixing of upper tropospheric and lower stratospheric air.

Figure 10. Potential vorticity maps for 12 UTC at θ = 375 K corresponding to the three 1962 Canberra flights in figure 6. It may be seen that the 19620131 (a) and 19620206 (c) flights correspond to incursions of low-PV air into the subarctic from the subtropics, whereas that of 19620201 (b) corresponds to an incursion of high-PV (vortex) air over the Bay of Biscay. The former have air like that seen by the ER-2 and WB57F in figures 7 and 9, while the latter has high ozone and low water characteristic of older air descended from the middle stratosphere.

Figure 11. An ozone-water scatterplot, redrawn from figure 3 of Roach (1962). Only the stratospheric points have been retained; points have been added from three ER-2 flights in January-February 1989 taken when the vortex was undisturbed (19890106, 19890112, 19890116) and from one flight when it was disturbed (19890207). All points in the range $350 < \theta < 400$ K have been plotted. Dots, 1962; crosses, 1989; the high water points correspond to disturbed conditions in each case.

Figure 12. Water and wind speed from the WB57F track on 19980507, flown isentropically at 370 K. The cross-section is on a line running from the right entrance towards the left exit of the subtropical jet stream maximum over the southern United States.

Figure 13. A scatterplot of the potential temperature at the tropopause, θ_{TROP}, versus latitude for the WB57F flights of 19980409, 19980501, 19980504, 19980511, 19990920 and 19990921. Note that for each flight θ_{TROP} is higher at the latitudes nearer the subtropical jet stream (i.e. further from the equator).

Figure 14. Water and methane measurements from the ER-2 flight of 19940327, between Hawaii (20°N, 158°W) and Fiji (18°S, 177°E). Even at $\theta > 440$ K, in the inner tropics the water is variable and has a shotgun relation with methane; the negative correlation elsewhere indicates the penetration of older air from midlatitudes into the outer tropics.

Figure 1

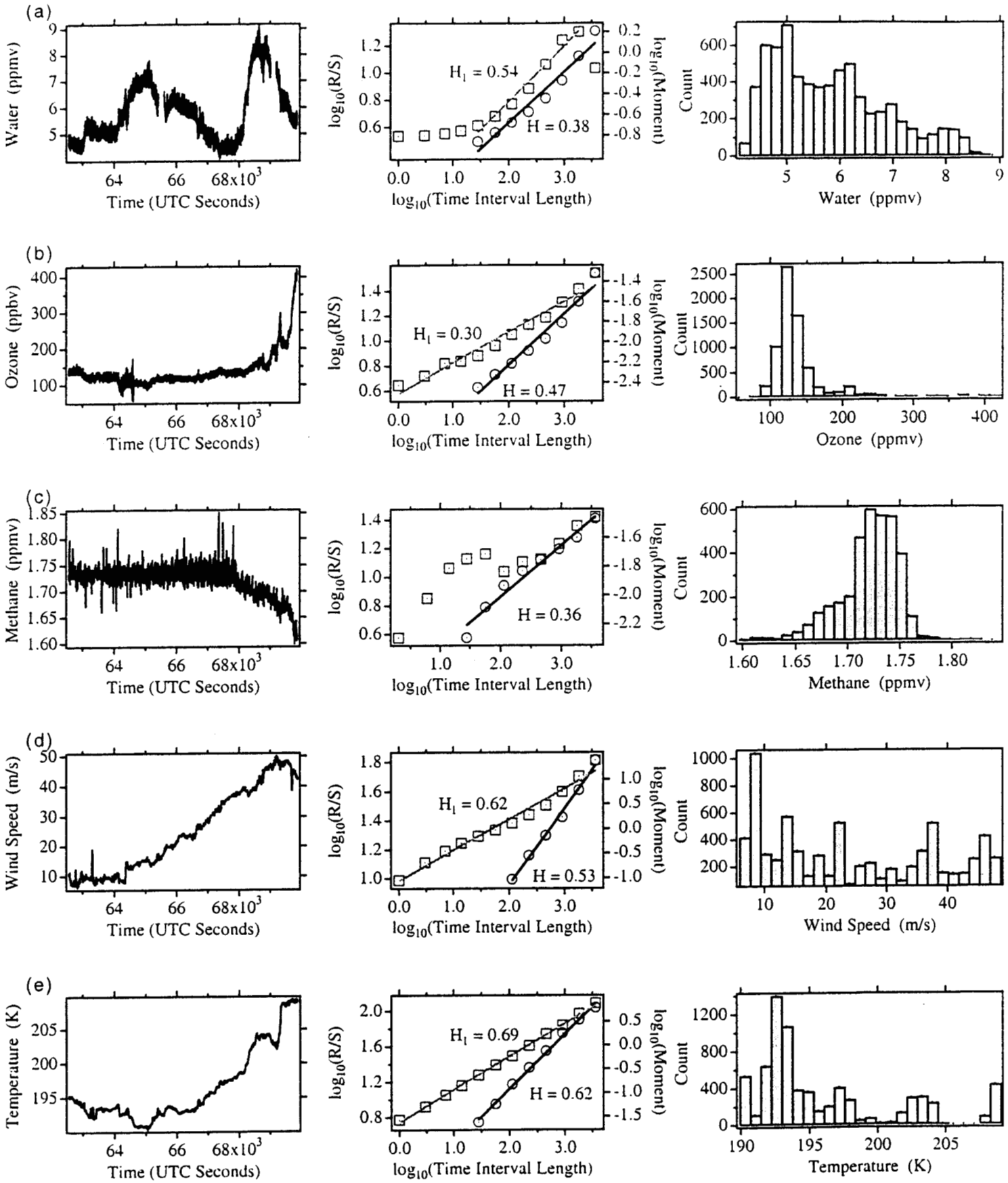

WAM WB57F 19980501 endchgalt-begindescent, 7314 sec

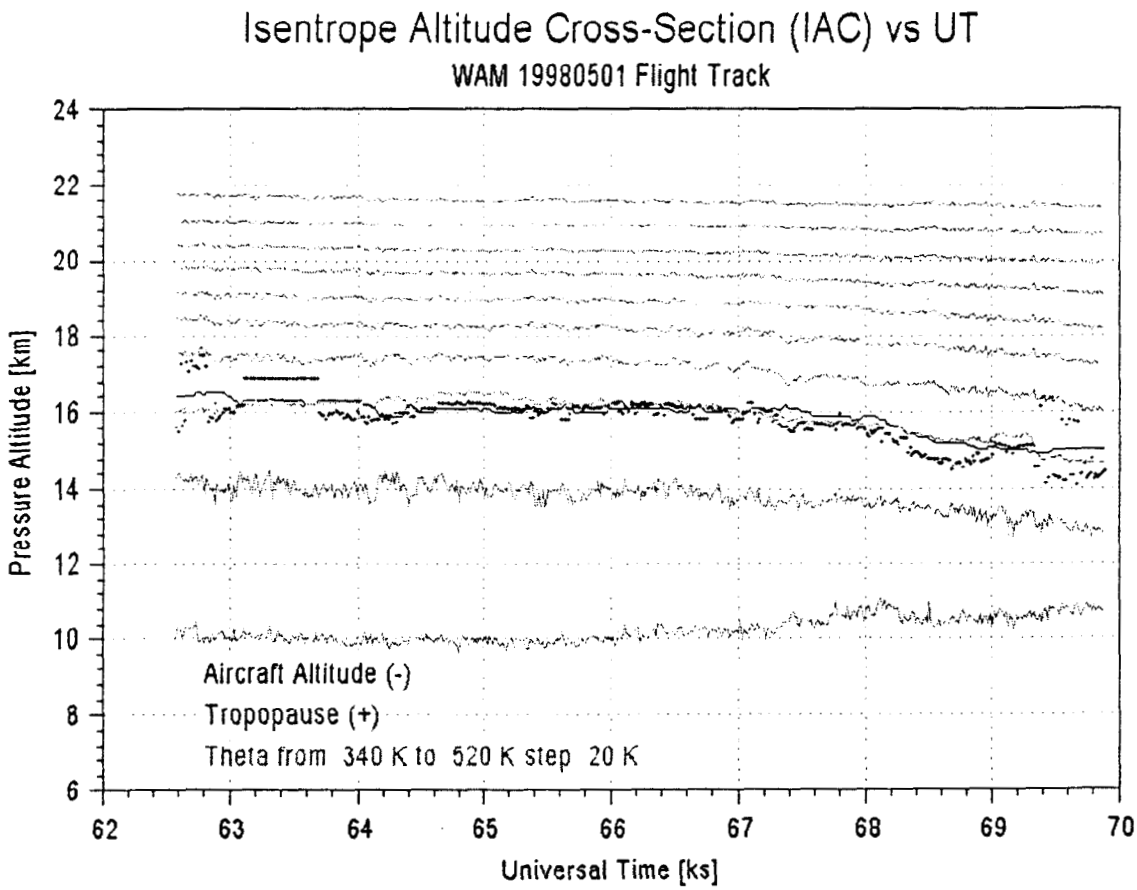
Isentrope Altitude Cross-Section (IAC) vs UT
WAM 19980501 Flight Track
Pressure Altitude [km]
24
22
20
18
16
14
12
10
8
6
62
63
64
65
66
67
68
69
70
Universal Time [ks]
Aircraft Altitude (-)
Tropopause (+)
Theta from 340 K to 520 K step 20 K

Figure 3

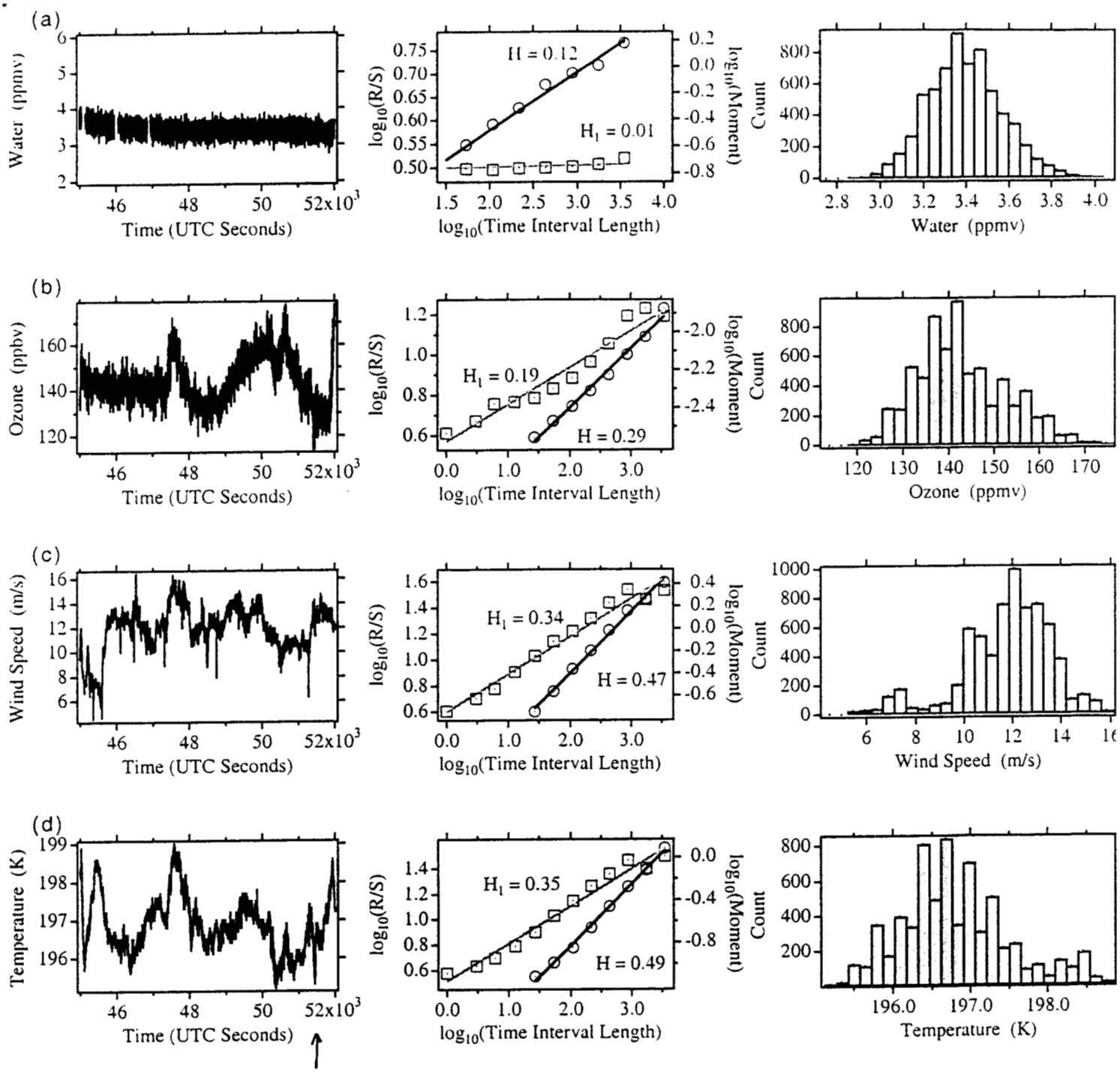

AAOE ER-2 19870814 45000-52000, 7001 sec

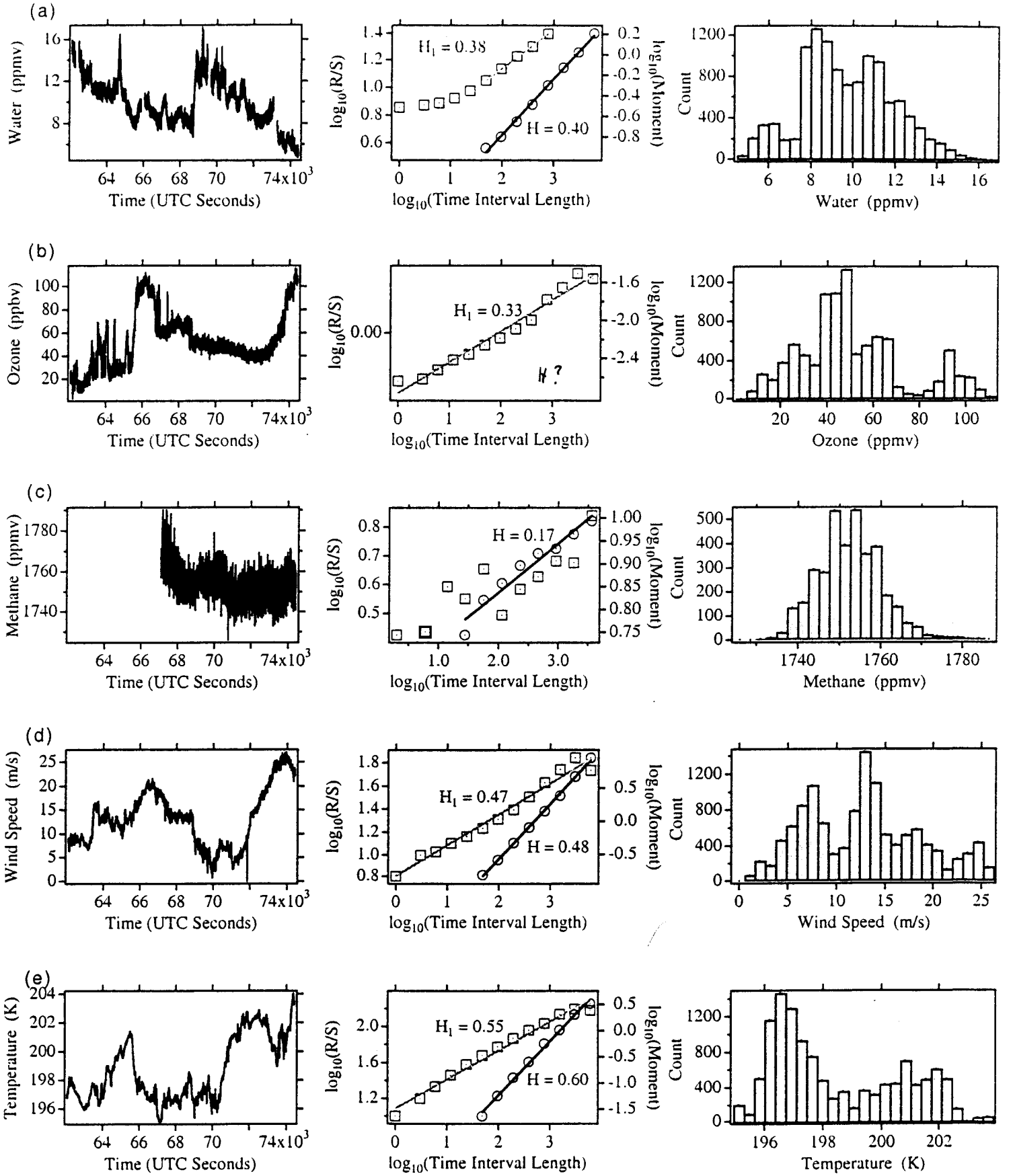

ACCENT WB57F 19990921 endascent-beginchgalt, 12323 sec

(a) Ozone

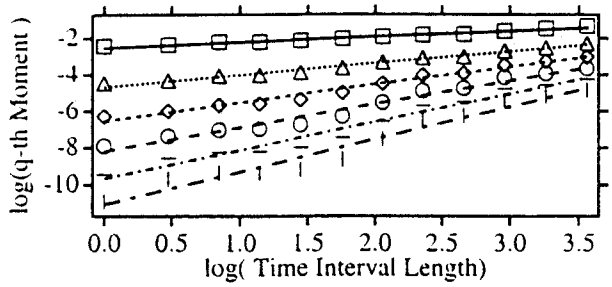

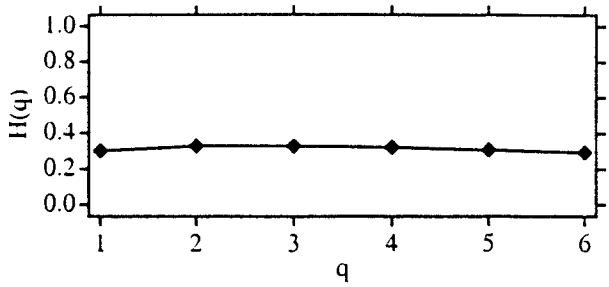

(b) Wind Speed

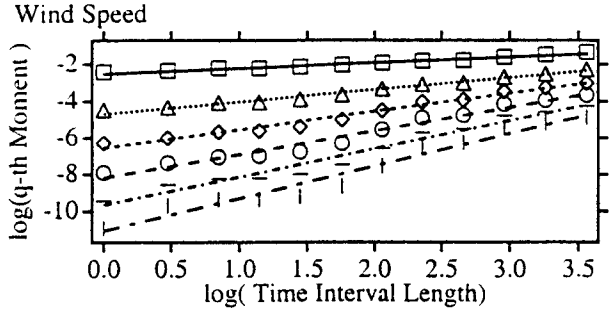

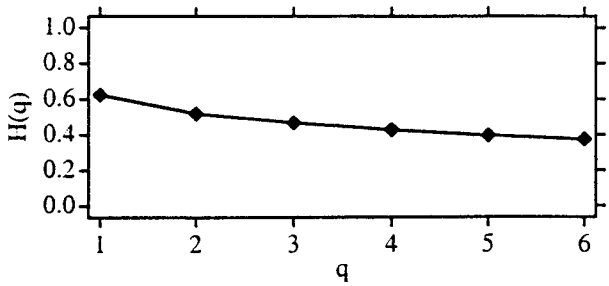

(c) Temperature

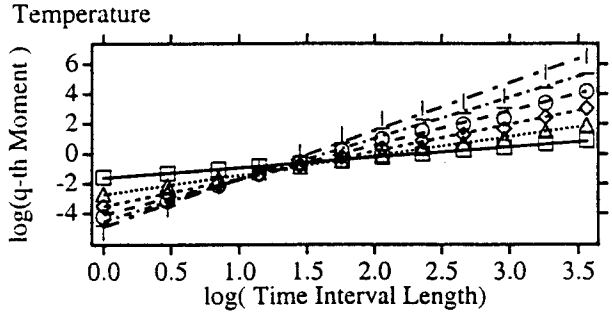

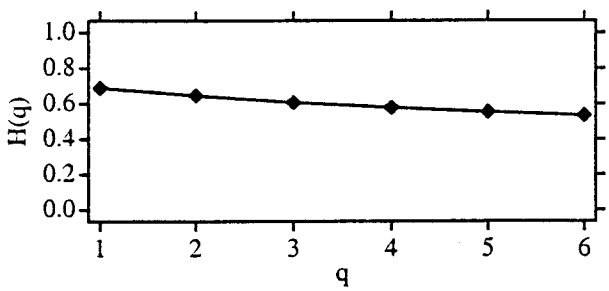

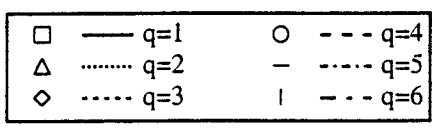

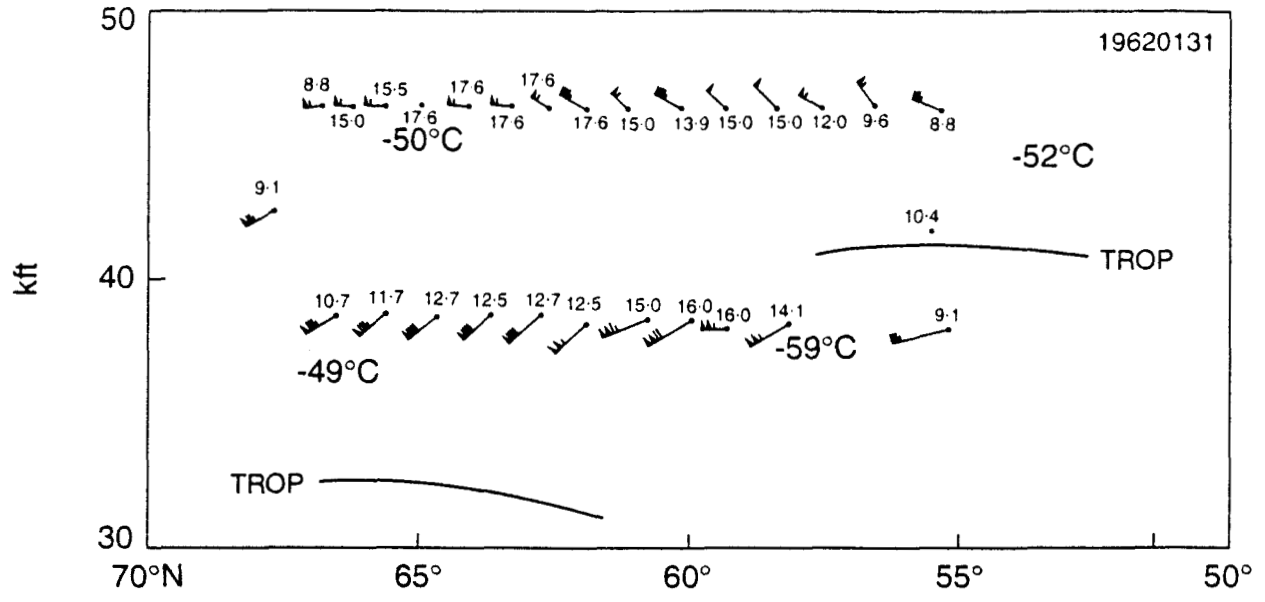
19620131
kft
50
40
30
70°N
65°
60°
55°
50°
-50°C
-52°C
-49°C
-59°C
TROP
TROP

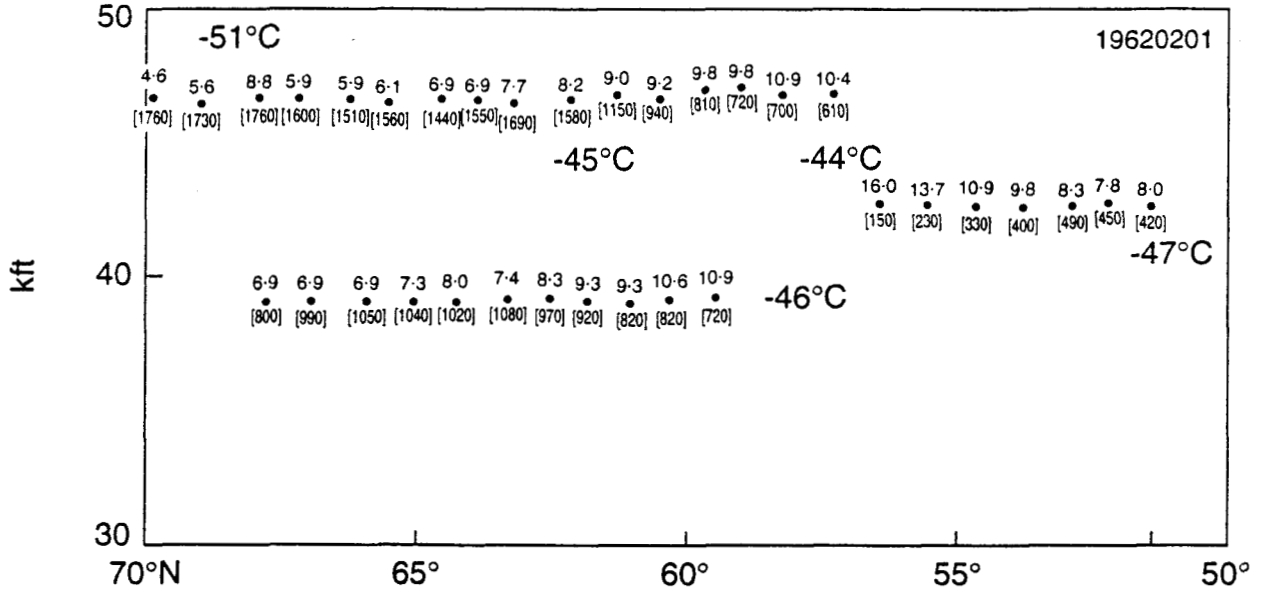
19620201
kft
50
40
30
70°N
65°
60°
55°
50°
-51°C
-45°C
-44°C
-47°C
-46°C

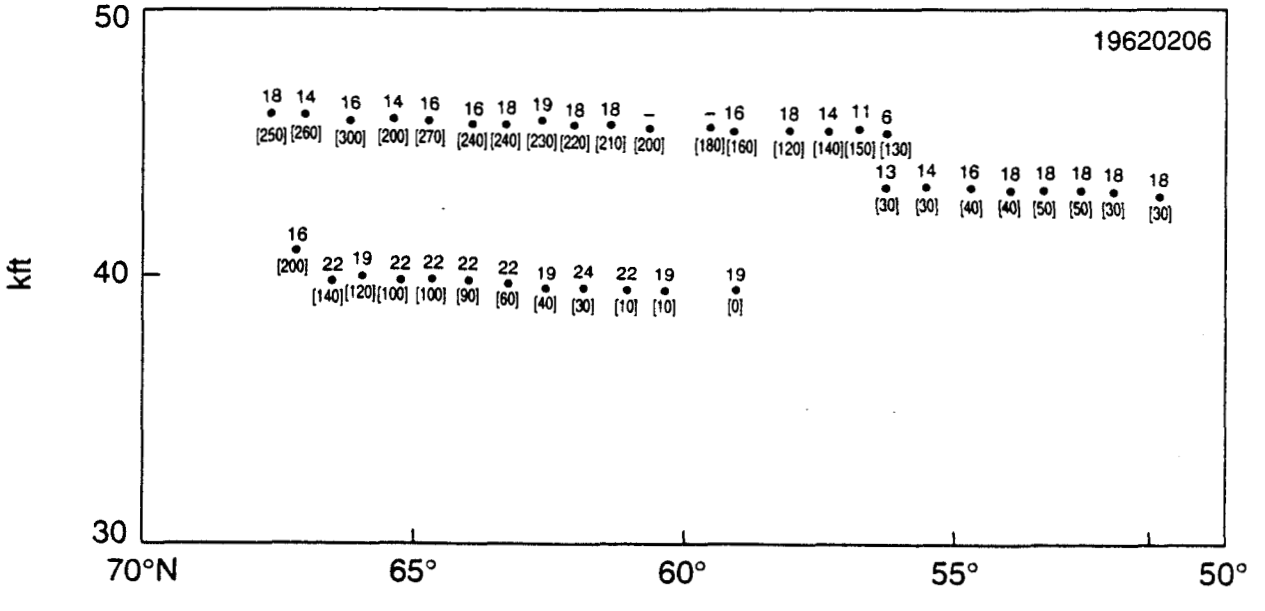
19620206
kft
50
40
30
70°N
65°
60°
55°
50°

Figure 7

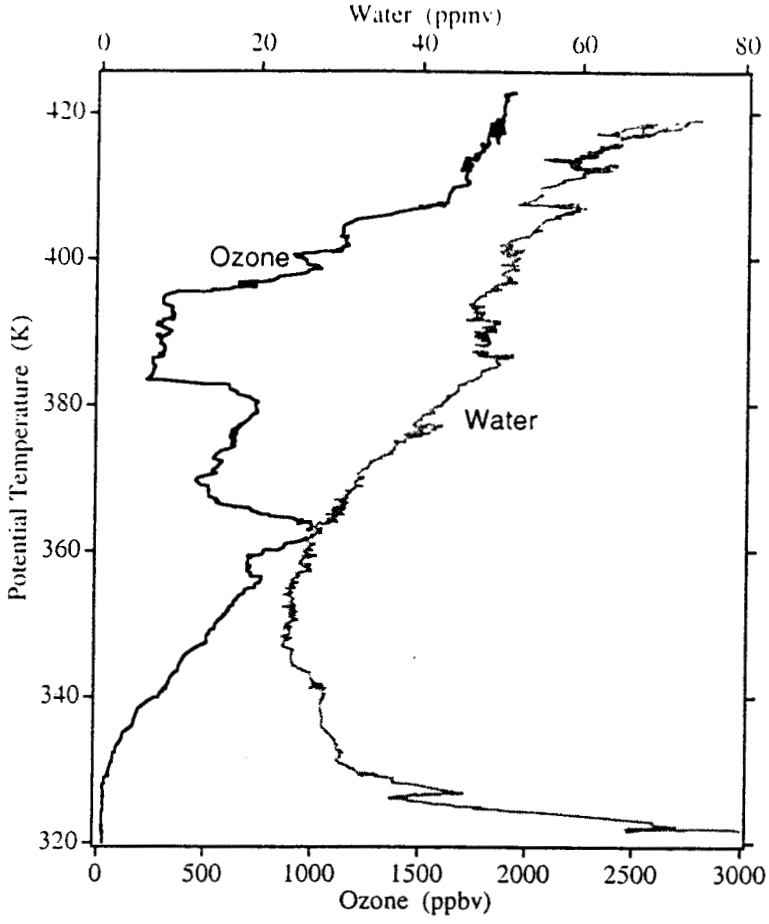

ER2 19890207 Ascent

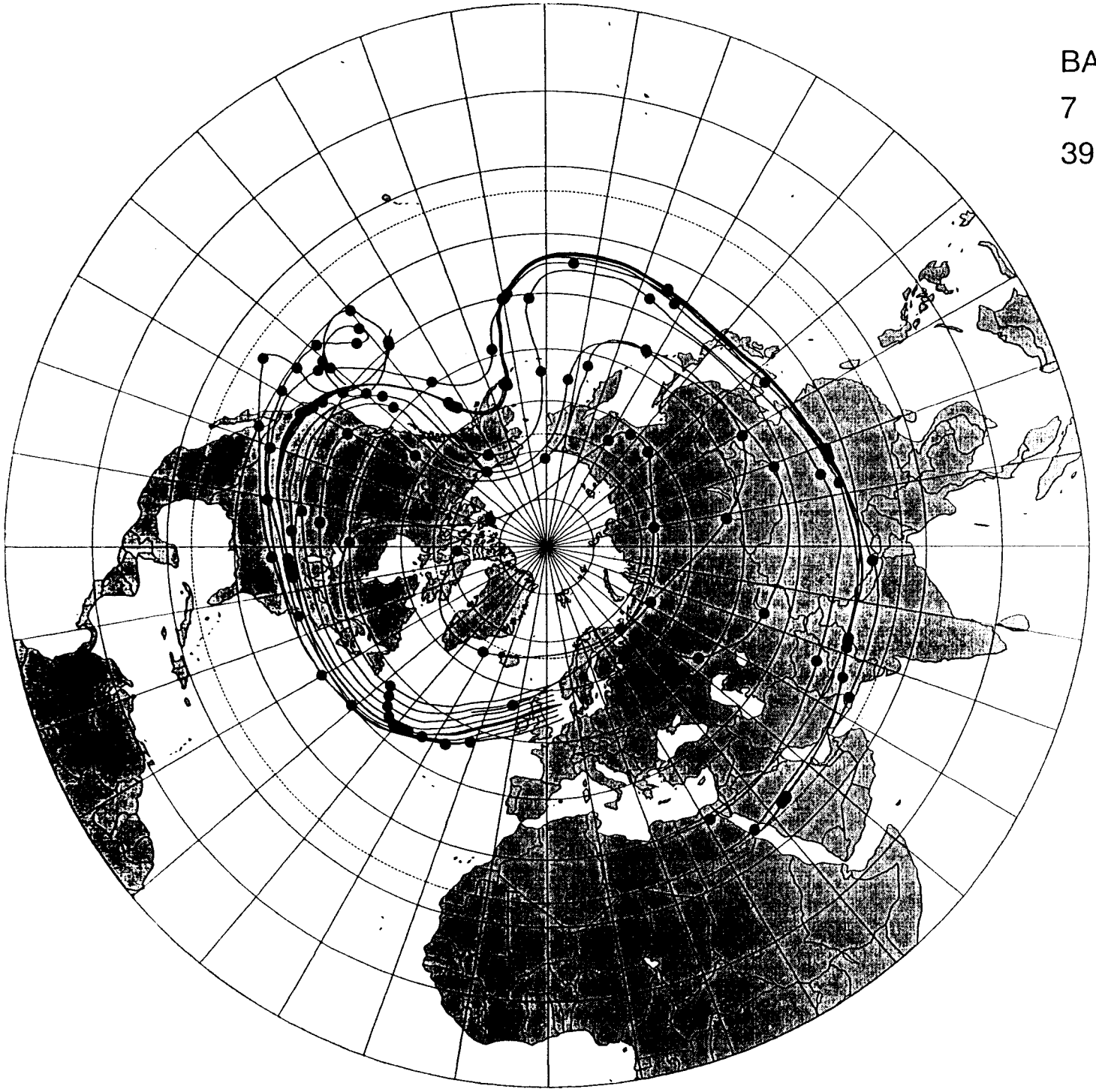

BACK TRAJECTORIES

7 2 89 6 Z

390 K

Figure 9

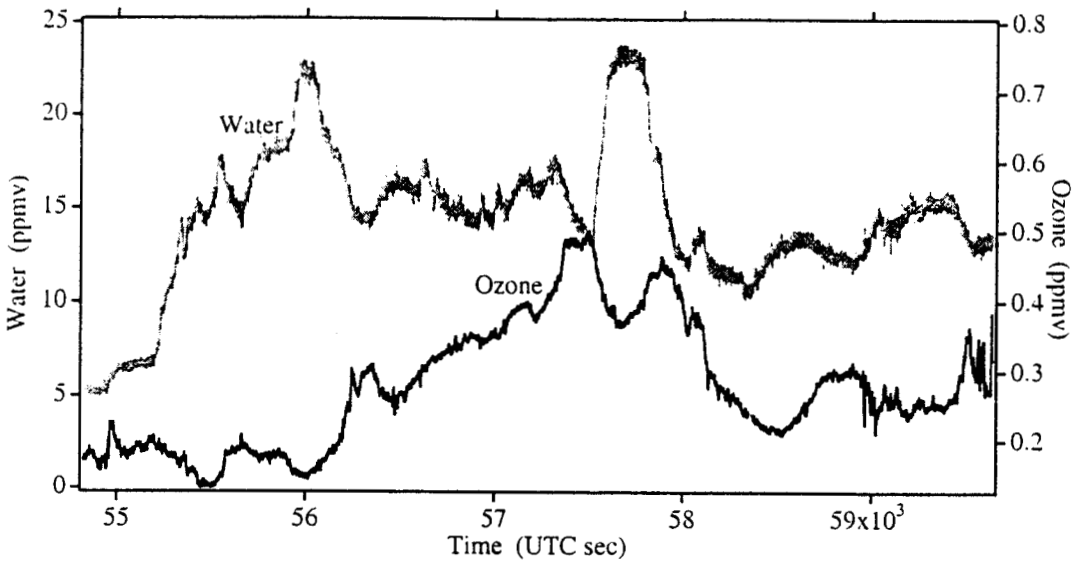
Water
Ozone
Water (ppmv)
Ozone (ppmv)
Time (UTC sec)
25
20
15
10
5
0
0.8
0.7
0.6
0.5
0.4
0.3
0.2
55
56
57
58
59x10^3

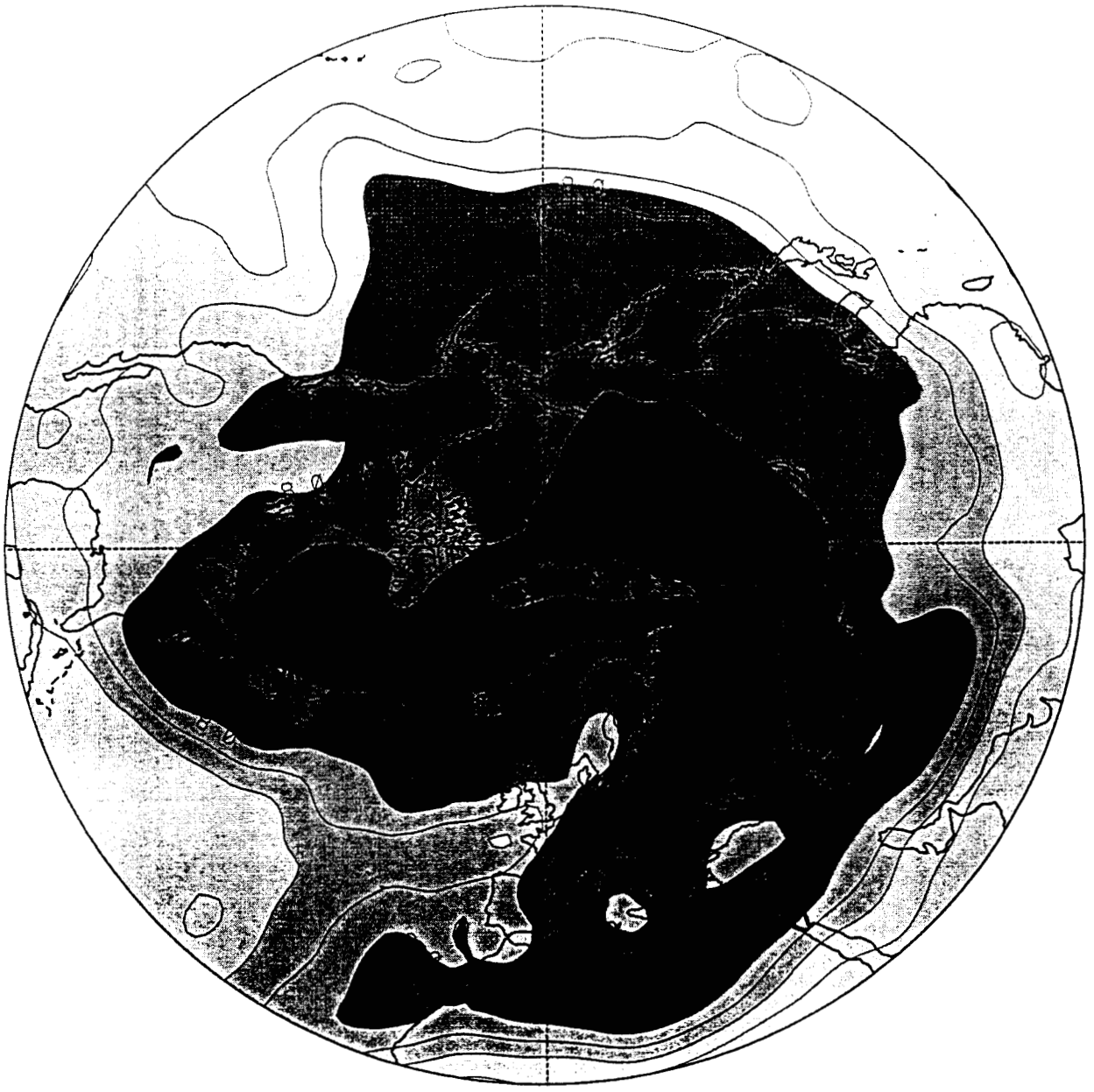

375 K IPV for 1962013112

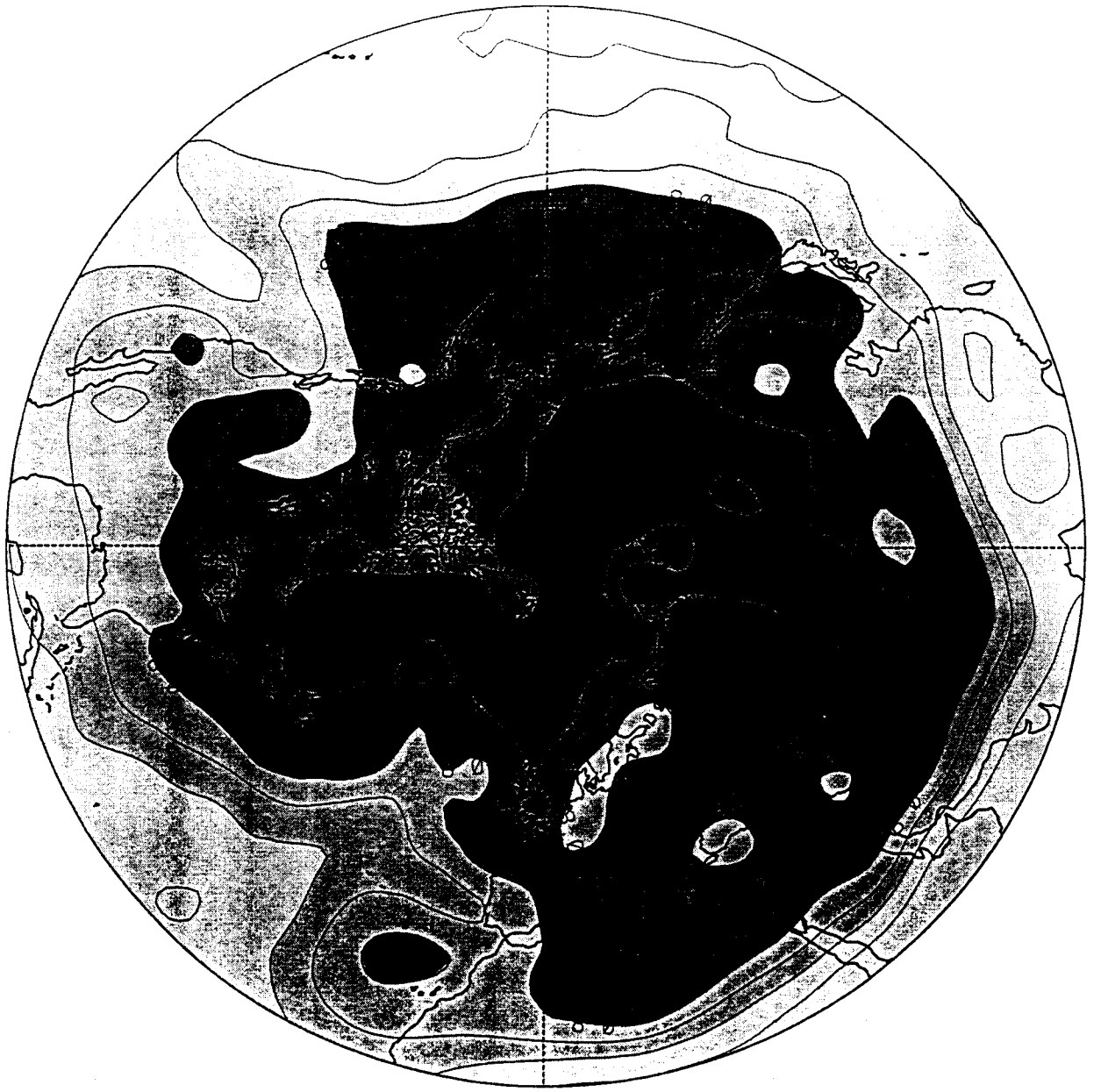

375 K IPV for 1962020112

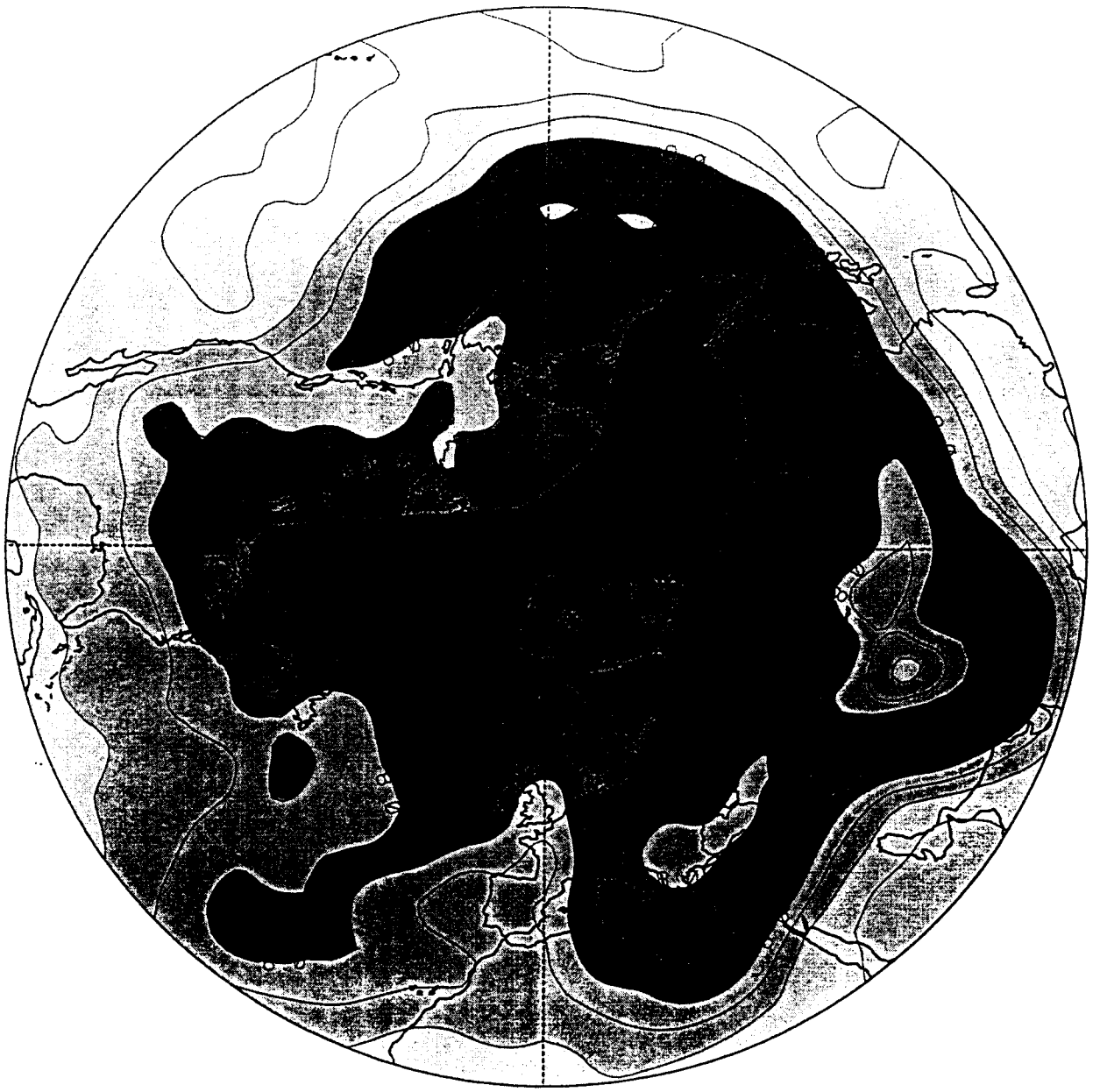

375 K IPV for 1962020612

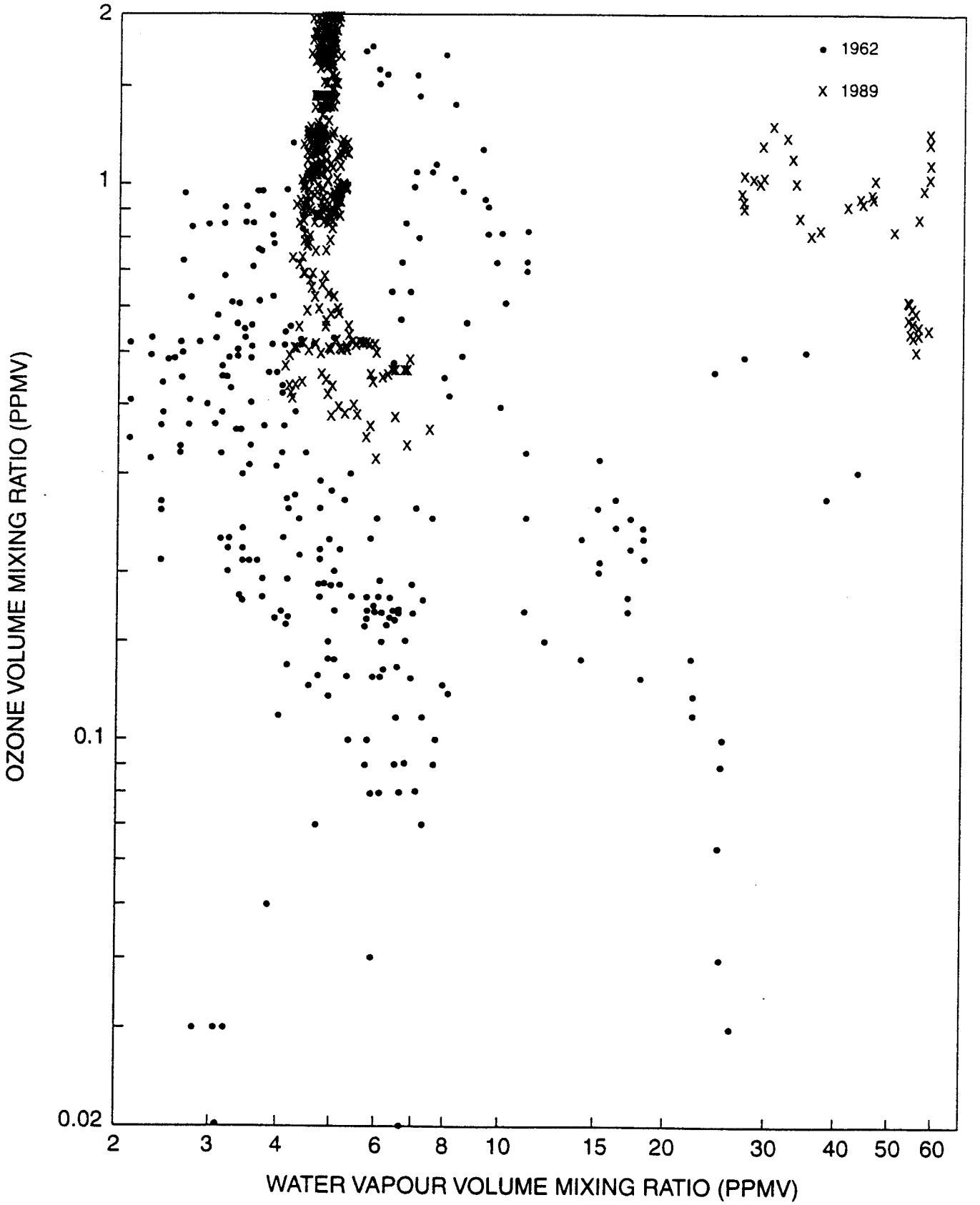
2
1
0.1
0.02
OZONE VOLUME MIXING RATIO (PPMV)
1962
1989
2
3
4
6
8
10
15
20
30
40
50
60
WATER VAPOUR VOLUME MIXING RATIO (PPMV)

Figure 12

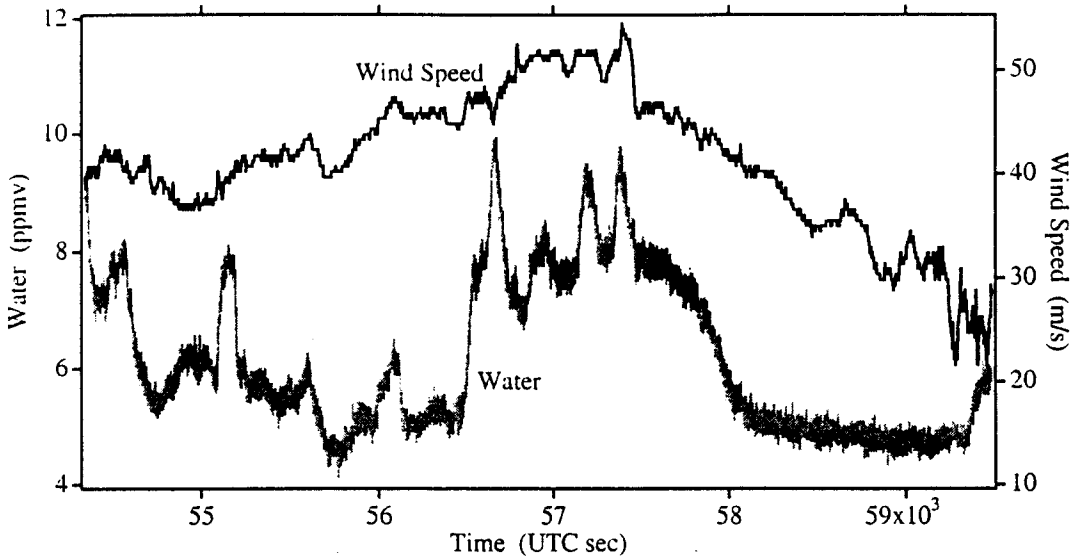
Wind Speed
Water
Water (ppmv)
Wind Speed (m/s)
Time (UTC sec)
12
10
8
6
4
50
40
30
20
10
55
56
57
58
59x10^3

Figure 14

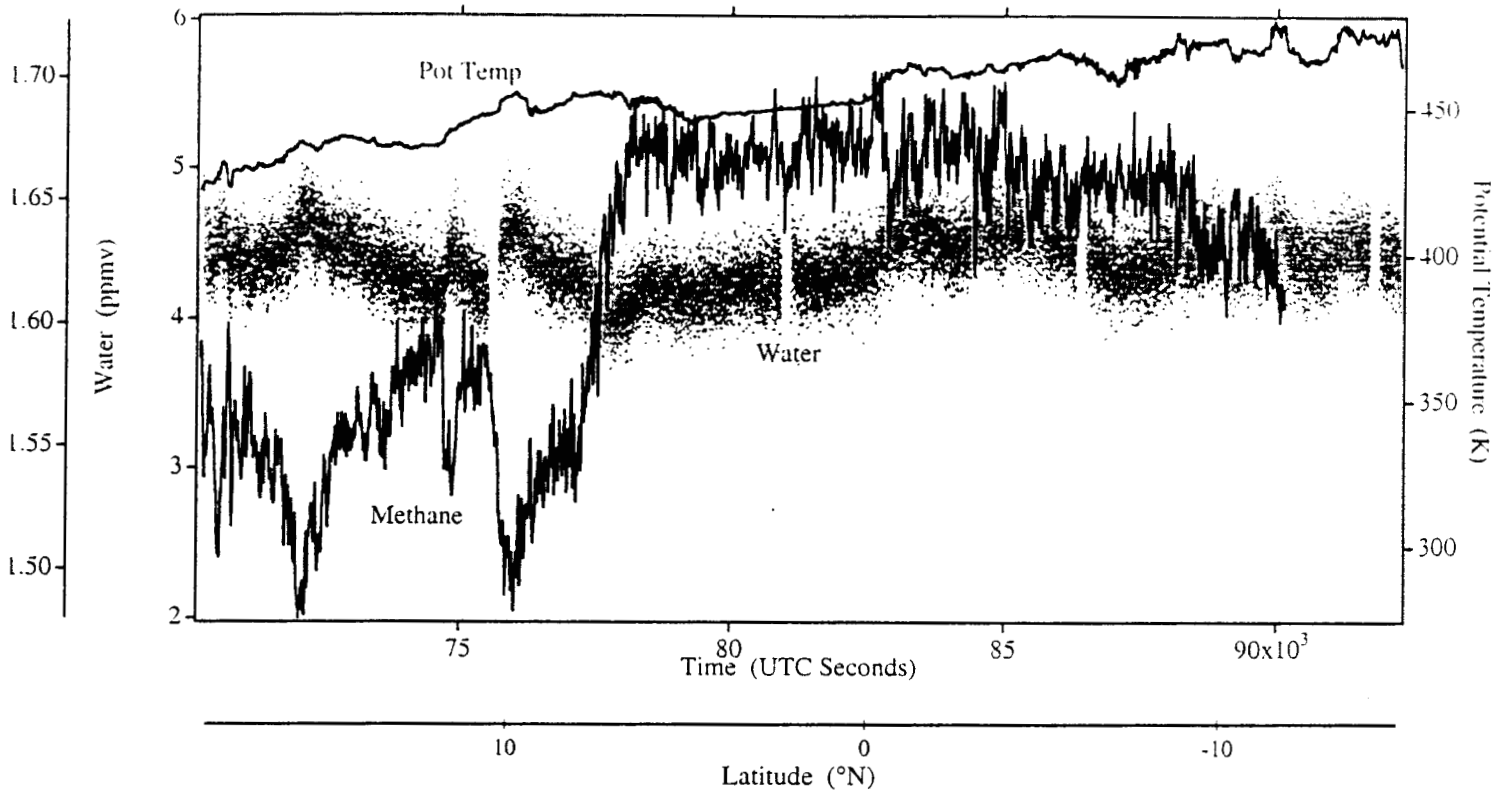

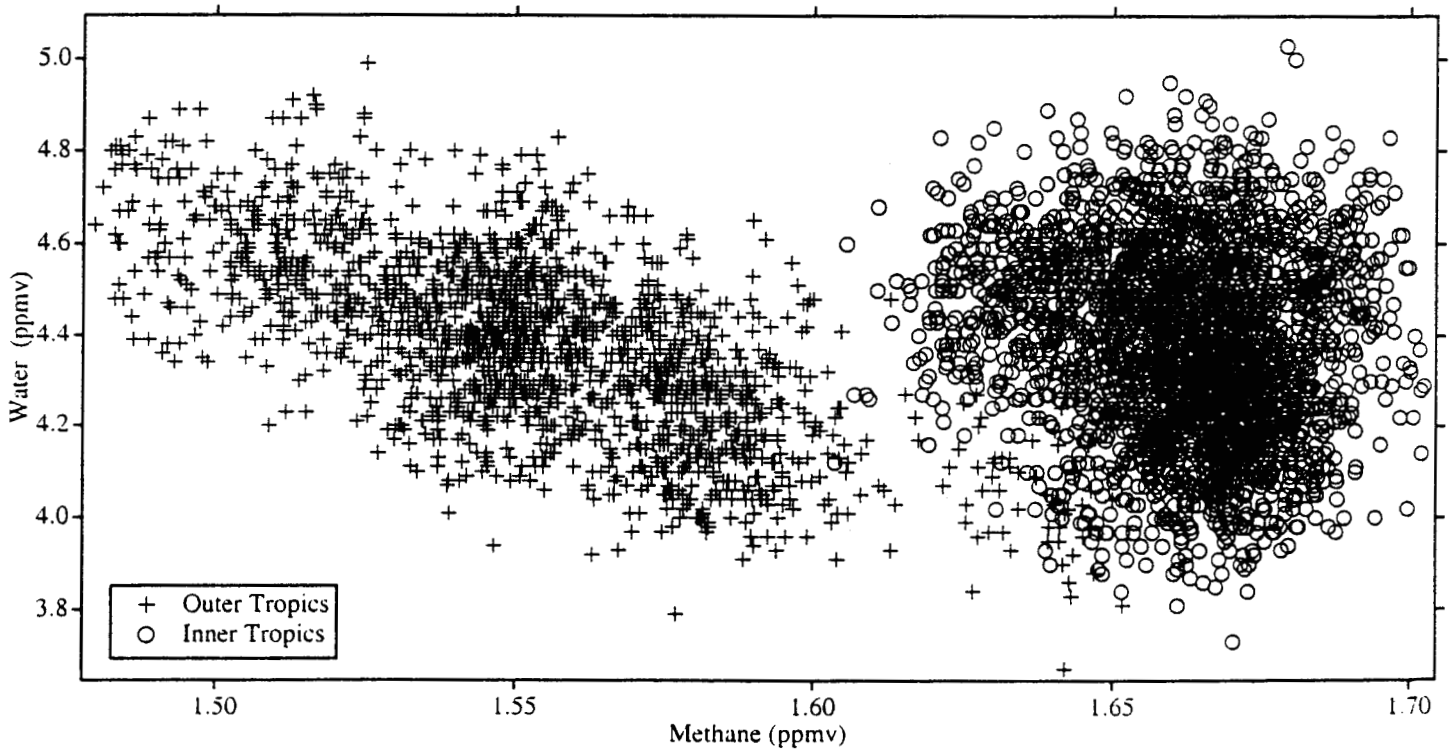

ASHOE ER-2 19940327 endascent-begindescent